



This project has received funding from the European Union's Seventh Programme for research, technological development and demonstration under grant agreement No [308417].



## New Directions in Seismic Hazard Assessment through Focused Earth Observation in the Marmara Supersite

Grant Agreement Number: 308417

co-funded by the European Commission within the Seventh Framework Programme

THEME [ENV.2012.6.4-2]

[Long-term monitoring experiment in geologically active regions of Europe prone to natural hazards: the Supersite concept]

### D3.4

## Deformation map obtained by applying InSAR technique to a sample L-Band SAR dataset

Project Start Date	1 November 2012
Project Duration	36 months
Project Coordinator /Organization	Nurcan Meral Özel / KOERI
Work Package Number	WP3
Deliverable Name/ Number	3.4
Due Date Of Deliverable	30 April 2014
Actual Submission Date	
Organization/Author (s)	BRGM/de Michele M., IREA/Manzo M., Boğaziçi Üniversitesi/Ergintav S.

Dissemination Level		
PU	Public	
PP	Restricted to other programme participants (including the Commission)	
RE	Restricted to a group specified by the consortium (including the Commission)	
CO	Confidential, only for members of the consortium (including the Commission)	

## TABLE OF CONTENTS

<b>1.CONTEXT .....</b>	<b>3</b>
<b>1.1 MARSITE PROJECT .....</b>	<b>3</b>
<b>2 L-BAND INSAR ON THE GANOS SACTION OF THE AFZ.....</b>	<b>4</b>
<b>2.1 TECTONIC CONTEXT OF THE STUDY AREA .....</b>	<b>4</b>
<b>2.2 L-BAND INSAR .....</b>	<b>8</b>
2.2.1 data acquisition and processing .....	8
2.2.2 Results.....	14
2.2.3 discussion .....	17
<b>BIBLIOGRAPHY .....</b>	<b>20</b>

### List Of Figures

<b>Figure 1.</b> The NAFZ. The red rectangle represents the Alos Palsar study area centered on the Ganos fault (after Janssen et al., 2009).....	5
<b>Figure 2a.</b> GPS velocities on the MARsite area (after Ergintav et al., 2012) .....	6
<b>Figure 2b.</b> GPS profiles on the Ganos section of the NAFZ (after Ergintav et al., 2012).....	7
<b>Figure 3.</b> Seismicity of the MARsite area -2006/2010- (after Ergintav et al., 2012).....	8
<b>Figure 4.</b> The shaded DEM from the Shuttle Radar Topography Mission. ....	13
<b>Figure 5.</b> The average signal coherence map. ....	14
<b>Figure 6.</b> Results (radians / year ) of the stacking procedure applied on 45 unwrapped interferograms. The colour scale goes from -0.8 cm/year to 2.7 cm/year. ....	15
<b>Figure 7.</b> Same as figure 4 but plotted in transparency on the shaded SRTM DEM. The colour scale is in radians / year ; it goes from -0.8 cm/year to 2.7 cm/year. ....	16
<b>Figure 8.</b> Stack of 45 interferograms with annotation about possible interpretation. The Ganos section of the NAFZ is plotted as a dashed red line. The colour scale is in radians / year ; it goes from -0.8 cm/year to 2.7 cm/year. ....	18

### List Of Tables

Table 1 . List of SAR data used in the present task .....	9
Table 2. List of interferograms generated and respective temporal baseline. The fence means that the interferogram was not used in the stacking procedure due to excessive noise. ....	11

MARSite (GA 308417) D3.4 Deformation map obtained by applying InSAR technique to a sample L-Band SAR dataset

# 1.Context

## 1.1 Marsite project

“The 1999 disastrous İzmit earthquake ( $M_w=7.4$ ) was not a surprise because westward migrating earthquakes that broke ~1000 km-long section of North Anatolian Fault (NAF) in a manner of falling dominos had already arrived nearby İzmit. Another large and destructive earthquake is now expected to occur further west along the North Anatolian fault under the Sea of Marmara, 20 km south of Istanbul, one of the most populous and rapidly growing cities of Europe. Historical documents going back to two millennia indicate that many destructive earthquakes stroke the city of Istanbul since the northern segment of the NAF under the Marmara Sea accommodates most of the plate motion between Anatolia and Eurasia. The probability of a large earthquake to strike Istanbul again is estimated to be about 65% over the next 30 years.” [from Marsite Project Introduction].

The present deliverable aims at showing the results retrieved from L band Interferometric Synthetic Aperture Radar (InSAR) measurements for the monitoring of Crustal Deformation in the Anatolian Fault Zone in the frame of the MARMARA SUPERSITE PROJECT "MARSITE".

We proposed to process SAR data made available through the CAT-1 ESA (European Space Agency) archives, acquired by the L-band radar sensor ALOS PALSAR, to retrieve surface displacements map on selected areas of the Anatolian Fault Zone (AFZ). In principle this exercise would allow us to map the spatial and temporal evolution of the present-day crustal deformation phenomena affecting the MARSite Area with high level of spatial details. The goal of this task is to assess whether InSAR L-Band data can be useful to evaluate the long-term behavior of active faults and eventual interactions between geologic structures, complementarily to GPS measurements and other in-situ observations. Besides, since InSAR maps motions of all nature occurring at the ground surface, we might expect to observe not only tectonic phenomena but also local subsidences due to land-sliding or sediment compaction.

In this specific task, mid-term monitoring (4 - 10 years) of the crustal deformation in the MARSite area will be investigated by using InSAR stacking approach. During the MARSite

MARSite (GA 308417) D3.4 Deformation map obtained by applying InSAR technique to a sample L-Band SAR dataset

project kick off meeting in Istanbul (2012), the WP3 group decided to select a specific section of the North Anatolian Fault Zone (NAFZ) to be used as a laboratory for L-band and C-band InSAR; the selected one is the Ganos section of the NAFZ, where our study is therefore concentrated.

Here in this deliverable, we aim at providing the L-band data acquisition frame, the data processing strategy, the preliminary results. A preliminary analysis of the results and some hints for further investigations are also highlighted. In a second step, we might aim at post-processing the results of this task and use them, if relevant, for characterizing the faults behavior. If possible, in a future step, the InSAR results will be jointly interpreted with the existing geodetic crustal deformation monitoring systems (Marmara Continuous GPS Network, with the complementary GPS surveys). Additionally, where possible and relevant, the InSAR results obtained in the frame of this task will be compared with the one made available through the Supersites Initiatives archives, acquired by new generation radar sensors (e. g. COSMO SKYMED and the future SENTINEL MISSION).

## **2 L-band InSAR on the Ganos section of the NAFZ**

### **2.1 Tectonic context of the study area**

The North Anatolian Fault (NAF), with a total length of about 1500 km, is one of the most active right-lateral strike-slip faults in the world. It defines the tectonic boundary between the Anatolian Plate and the Eurasian Plate in northern Turkey, accommodating ~14–30 mm/yr of relative plate motion between the two plates (fig. 1). The Gazikoy–Saros segment (the Ganos fault, GF) is the onshore segment of the northern strand of the NAF between the Marmara Sea and the Gulf of Saros. It was last ruptured in 1912 with a  $M_s=7.4$  earthquake that broke the entire inland segment of the fault, a length of about 50 km, and produced a right-lateral strike-slip component of at least 3 m. Other large historical earthquakes that have been attributed to the Ganos fault occurred in A.D. 824, 1343, 1509 and 1766 (e. g. Reilinger et al., 2000; Meade et al., 2002; Motagh et al., 2007; Janssen et al., 2009; Megraoui et al., 2012 ; Ersen Aksoy et al., 2010).

The GF forms a 45 km long linear fault system and represents the link between the northern strand of the NAFZ in the Sea of Marmara and the North Aegean Trough where slip partitioning results in branching of the fault zone (e.g. Barka and Kadinsky-Cade, 1988; Okay et al., 1999).

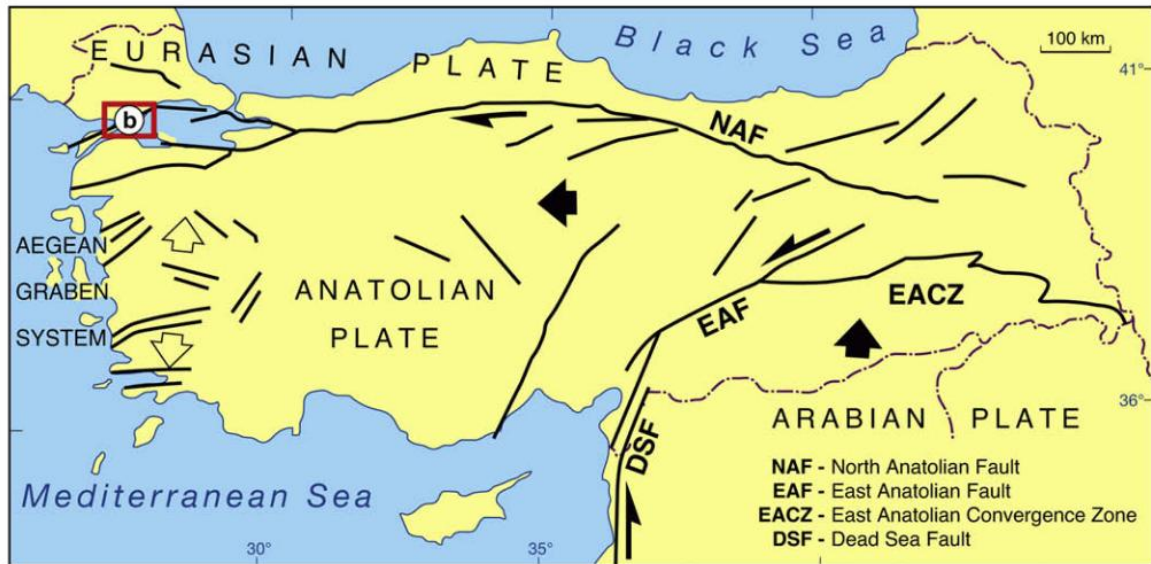


Figure 9. The NAFZ. The red rectangle represents the Alos Palsar study area centered on the Ganos fault (after Janssen et al., 2009).

The GF consists of several sub-parallel faults, which are separated by less than 1 km (Okay et al., 2004). The trace of the fault is clearly discernable on the SRTM DEM image with its northeastern part being bounded by the Ganos Mountains. A dominant right-lateral strike-slip motion became active toward the end of the Miocene and formed the Ganos Mountains due to transpressional uplift (Okay et al., 1999). Since the latest Miocene the total accumulated right-lateral displacement is in the order of 40 km (Okay et al., 1999). At present, the GF accommodates fault-normal convergence at a rate of  $1.1 \pm 0.4$  mm/yr (fig. 2a, b) (Okay et al., 2004; Ergintav et al., 2012). Tuysuz et al. (1998) interpreted the apparent lack of seismicity for magnitudes larger than 3 along the GF as an indication for a locked fault segment that slips only during large earthquakes. Recent interferometry and GPS measurements estimated a fault locking depth in the range of 8-17 km (Motagh et al., 2007, Ergintav et al., 2012).



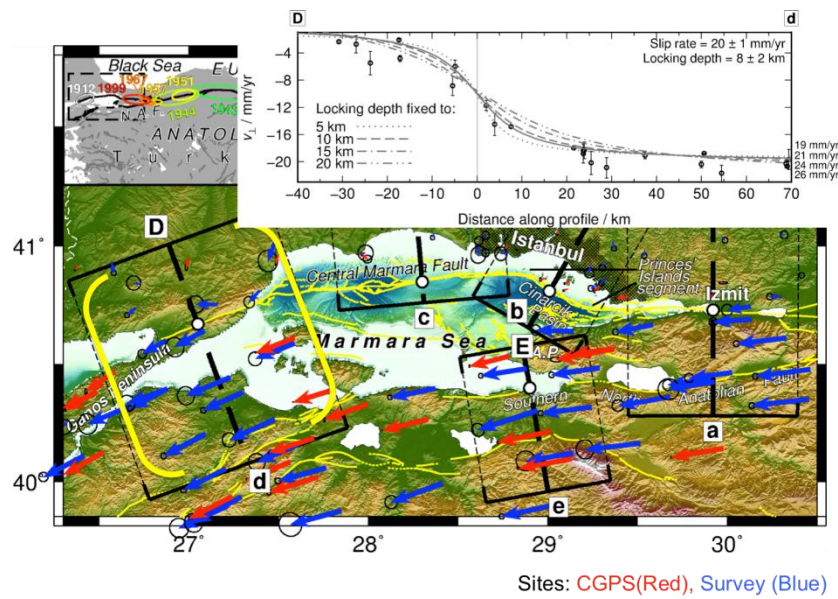
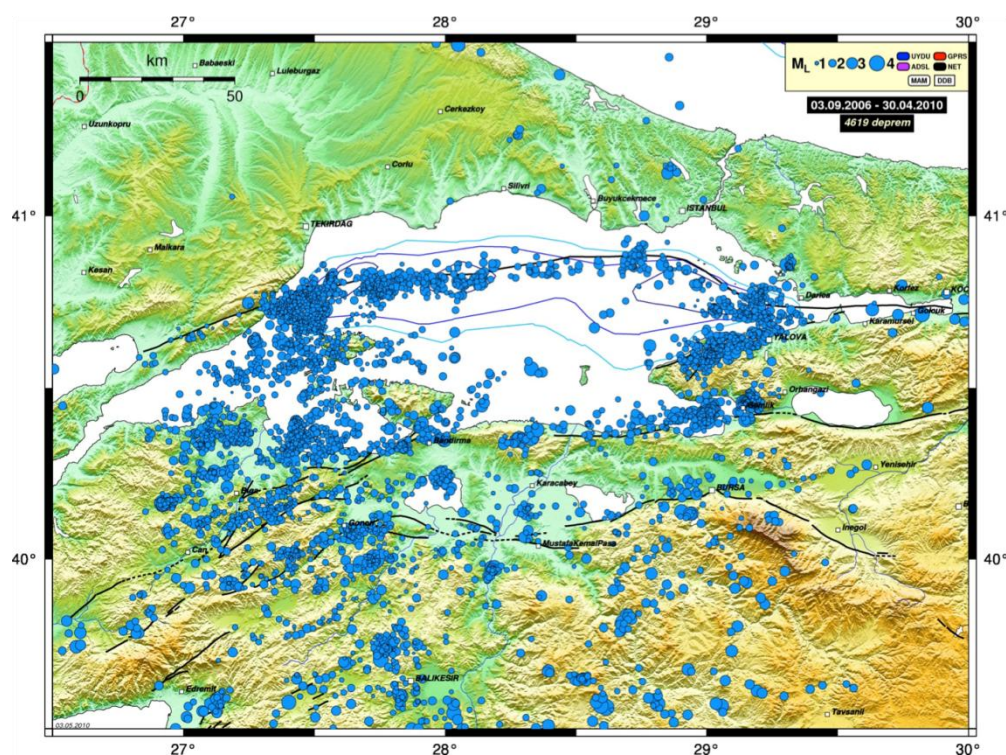


Figure 2b. GPS profiles on the Ganos section of the NAFZ (after Ergintav et al., 2012).

Based on sea floor observations, Armijo et al. (2005) suggested that the rupture even extended into the Marmara Sea. The last earthquake at the GF ( $M > 4$ ) occurred in 1985 in the Ganos Mountains with a reverse faulting mechanism on a NE striking fault plane (Janssen et al., 2009).



ALOS PALSAR InSAR can map ground deformation at a spatial resolution of tens of meters with subcentimeter precision in the line-of-sight direction (LOS) of the satellite (e.g., Massonnet and Feigl, 1998). We acquired all available ALOS PALSAR archived data for the Ganos section of the NAFZ. We chose to process the ascending orbit ALOS PALSAR acquisitions as there are only ascending data on the archive catalogue. Besides, the satellite path orientation with respect to the fault orientation is optimal to obtain a suitable InSAR LOS sensitivity to strike-slip surface movement parallel to the NAFZ at the Ganos section. The shallow creep signal is expected to range from ~0 to 1.5 cm/yr. Atmospheric delays in the radar images of the interferometric pair could mask this kind of signal in a single interferogram (Puysségur et al., 2007; Zebker et al., 1997).

data	mode	orbit	Look angle
07/07/2007	FBS	ascending	38,7°
07/10/2007	FBS	ascending	38,7°
08/04/2008	FBD	ascending	38,7°
24/08/2008	FBS	ascending	38,7°
09/10/2008	FBS	ascending	38,7°
24/02/2009	FBD	ascending	38,7°
12/07/2009	FBS	ascending	38,7°
27/08/2009	FBS	ascending	38,7°
12/10/2009	FBS	ascending	38,7°
30/05/2010	FBS	ascending	38,7°
15/07/2010	FBS	ascending	38,7°
30/08/2010	FBS	ascending	38,7°
15/01/2011	FBD	ascending	38,7°

Table 3 . List of SAR data used in the present task

To reduce atmospheric influence on the interferometric phase, we used a stacking methodology (in this study we do not use the widely known small-baseline subset, SBAS—Berardino et al., 2002). We used the stacking method as implemented in the GAMMA software (Wegmüller et al., 2009; de Michele et al., 2011). The starting point was a set of 13 SLCs ALOS PALSAR images that were combined to calculate 66 differential interferograms with a perpendicular baseline of less than 500 m. We encountered a co-registration

problem, probably due to a large Doppler difference, on one image (2007/07/07) therefore we only used 12 images in the stack.

Topographic contributions to the interferometric phase were calculated for each interferogram using the Shuttle Radar Topography Mission (SRTM) 90-m digital elevation model (DEM) (fig. 4) and subtracted from the interferograms. The SRTM DEM was also used in a later stage to project the results into a geographic orthoprojection. From the 66 initial differential interferograms (tab. II), a subset of 41 high-signal-coherence interferograms was selected based on visual analysis. We chose a signal coherence  $\geq 0.6$  on at least  $\sim 75\%$  of the dataset (fig 5). We used the GAMMA Minimum Cost Flow (MCF) algorithm (Costantini and Rosen, 1999; Werner et al., 2002) to unwrap the selected interferograms. For each interferogram, the unwrapping step, performed at the full resolution grid, was improved using a phase reference model obtained by unwrapping the corresponding multiple-look interferogram.

date (Master)	date (Slave)	time spam (days)
20071007	20080408	183.9986
#20071007	20080824	321.9983
#20071007	20081009	367.9989
20071007	20090224	506.0004
20071007	20090712	644.0011
20071007	20090827	690.0013
20071007	20091012	736.0014
20071007	20100530	966.0007
20071007	20100715	1012.0004
20071007	20100830	1058.0000
20071007	20110115	1195.9984
#20080408	20080824	137.9997
#20080408	20081009	184.0004
20080408	20090224	322.0018
20080408	20090712	460.0026
20080408	20090827	506.0027
20080408	20091012	552.0028
20080408	20100530	782.0021
20080408	20100715	828.0018
20080408	20100830	874.0014
#20080408	20110115	1011.9998
20080824	20081009	46.0006
20080824	20090224	184.0021
20080824	20090712	322.0028

MARSite (GA 308417) D3.4 Deformation map obtained by applying InSAR technique to a sample L-Band SAR dataset

#20080824	20090827	368.0030
20080824	20091012	414.0031
#20080824	20100530	644.0024
#20080824	20100715	690.0021
#20080824	20100830	736.0017
#20080824	20110115	874.0001
20081009	20090224	138.0015
20081009	20090712	276.0022
#20081009	20090827	322.0024
20081009	20091012	368.0025
#20081009	20100530	598.0018
#20081009	20100715	644.0014
#20081009	20100830	690.0011
#20081009	20110115	827.9995
20090224	20090712	138.0007
20090224	20090827	184.0009
20090224	20091012	230.0010
#20090224	20100530	460.0003
#20090224	20100715	506.0000
20090224	20100830	551.9996
#20090224	20110115	689.9980
20090712	20090827	46.0002
20090712	20091012	92.0003
20090712	20100530	321.9996
20090712	20100715	367.9992
20090712	20100830	413.9988
20090712	20110115	551.9973
20090827	20091012	46.0001
20090827	20100530	275.9994
#20090827	20100715	321.9991
20090827	20100830	367.9987
#20090827	20110115	505.9971
20091012	20100530	229.9993
20091012	20100715	275.9990
20091012	20100830	321.9986
20091012	20110115	459.9970
20100530	20100715	45.9997
20100530	20100830	91.9993
20100530	20110115	229.9977
20100715	20100830	45.9996
20100715	20110115	183.9980
#20100830	20110115	137.9984

**Table 4. List of interferograms generated and respective temporal baseline. The fence means that the interferogram was not used in the stacking procedure due to excessive noise.**

The phase reference model was then resized to the original pixel resolution (at the full resolution grid).

For each pixel, the unwrapped phase value was computed from the complex valued interferogram under the assumption that the phase values in the resized model correspond to the correct unwrapped phase within the interval  $\pm\pi$ . The resulting unwrapped phase meets the condition that rewrapping of the unwrapped phase results in exactly the phase of the complex interferogram, except for a constant offset which can be defined through the phase indicated for the reference location (Werner et al., 2002).

The atmospheric phase delay was also estimated. We observe that, depending on atmospheric conditions, the path delay might have an altitude dependence caused by changes in the atmospheric water vapor and pressure profiles between the acquisitions of the interferometric image pairs (e.g., Doin et al., 2009). In the study region, the atmospheric phase delay is not as exacerbated by extraordinary relief as has been reported elsewhere (e.g., Elliot et al., 2008). To find subtle signals due to land displacements, we used GAMMA to determine the linear regression coefficients of the residual phase with respect to height in the unwrapped interferograms. We used the DEM (in radar geometry) to generate the phase model of the height-dependent atmospheric phase delay for each unwrapped interferogram. Each phase model was then subtracted from the corresponding single unwrapped interferogram.

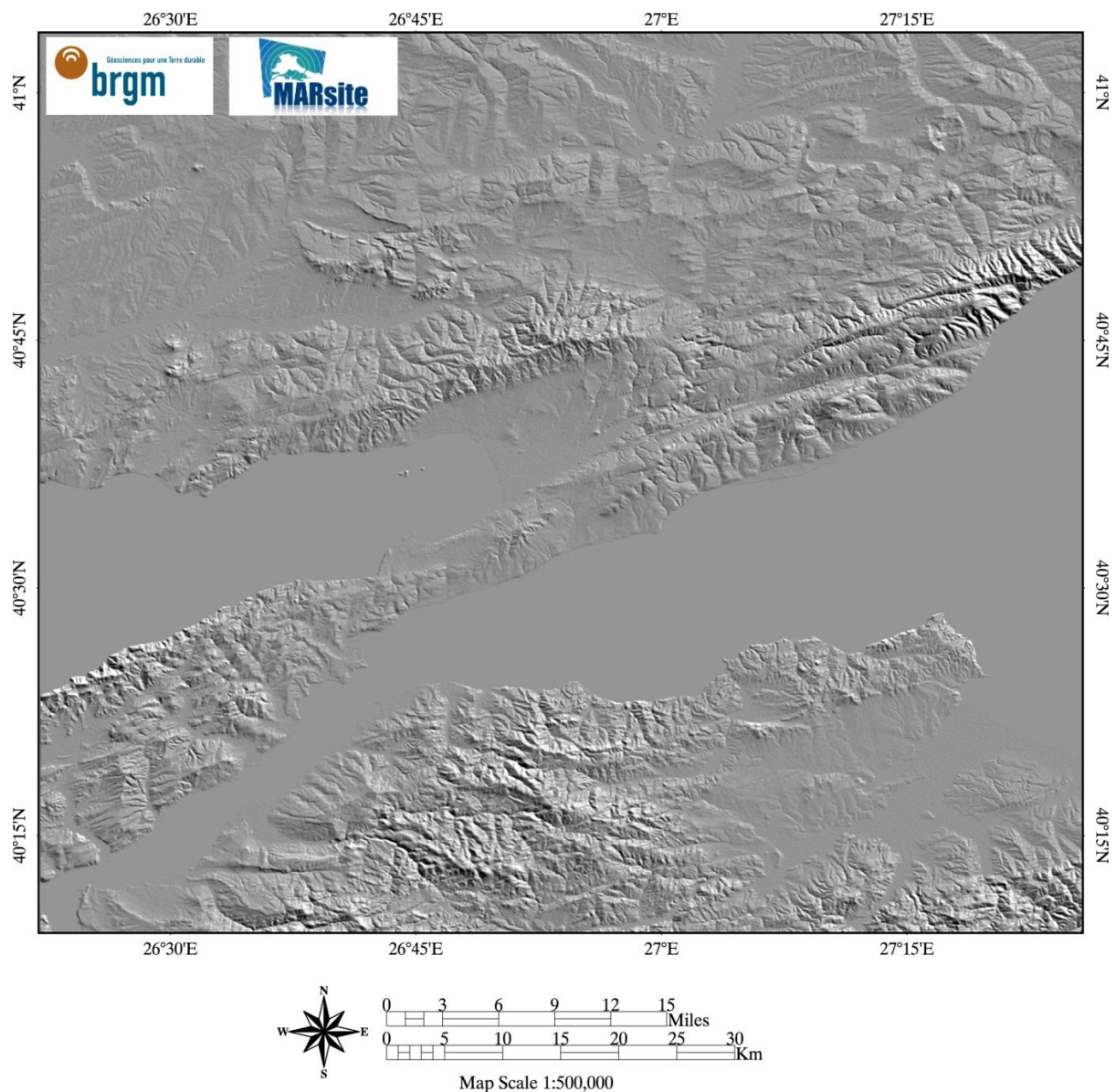


**Figure 12. The shaded DEM from the Shuttle Radar Topography Mission.**

Then, the stacking algorithm was used to estimate the linear rate of differential phase using the set of unwrapped differential interferograms, to derive a time averaged linear velocity map over the study area. The stacking algorithm uses the individual interferogram phases weighted by the time interval in estimating the phase rate. The underlying assumption is that atmospheric statistics are stationary for the set of interferograms while land displacement is not. No a priori models of surface displacement were used in any of the processing steps described above.

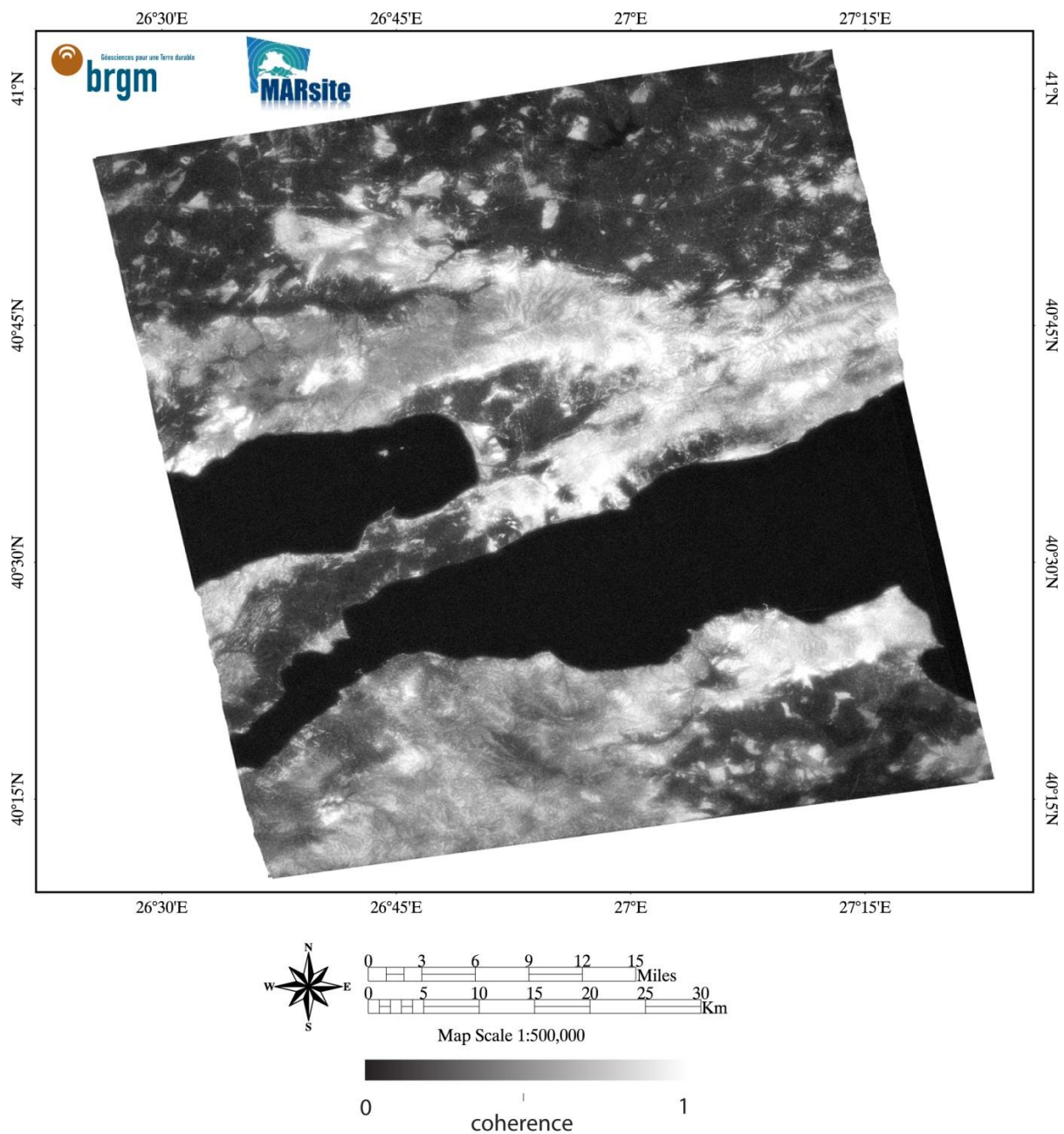


Figure 13. The average signal coherence map.

### 2.2.2 Results

One result of this analysis is the SAR phase linear evolution with time calculated from 2007 to 2011 and measured in the LOS direction of the sensor (fig. 6).

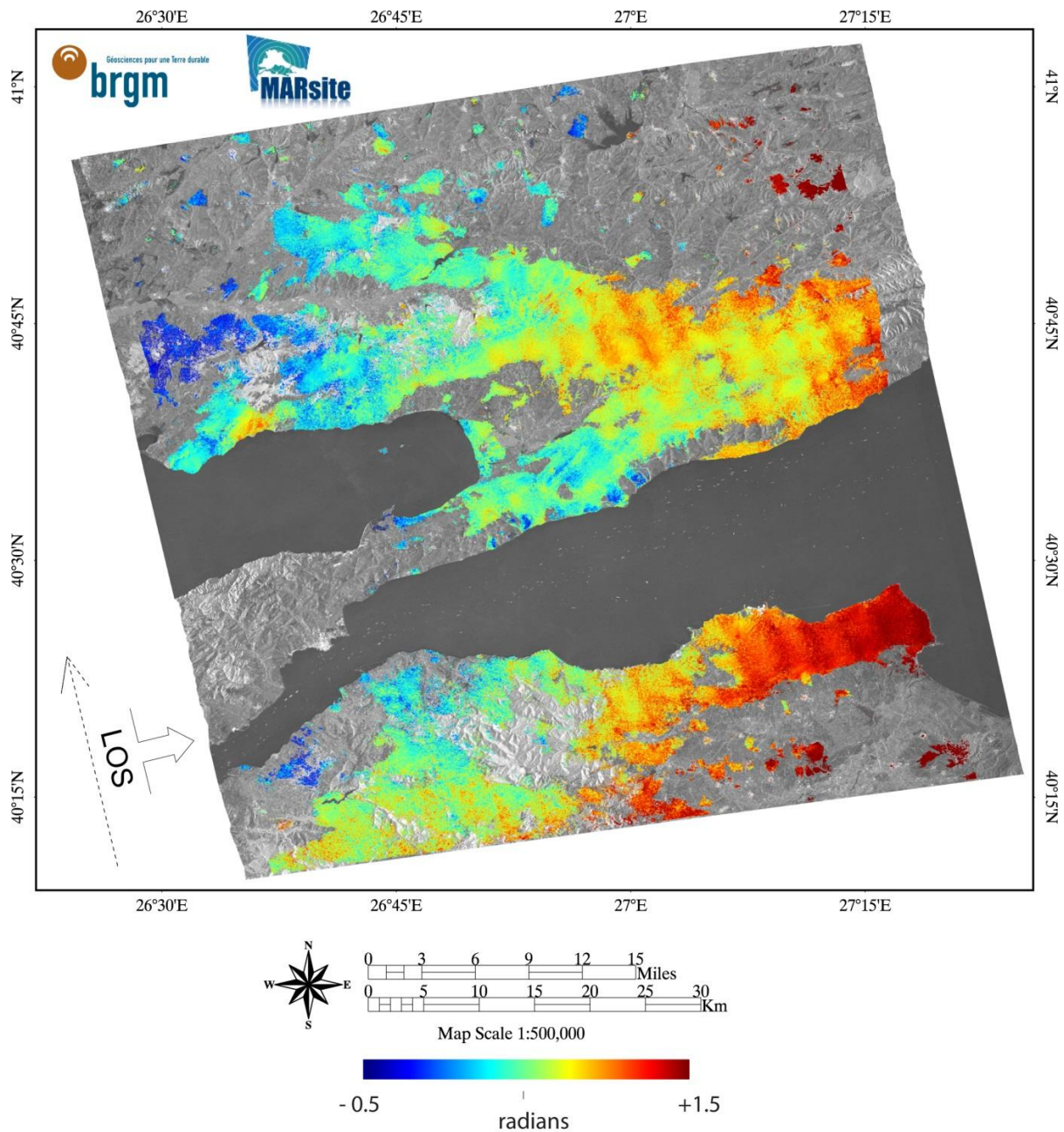


Figure 14. Results (radians / year ) of the stacking procedure applied on 45 unwrapped interferograms. The colour scale goes from -0.8 cm/year to 2.7 cm/year.

There is not a clear bimodal distribution of the surface displacement consistent with dextral shear. Therefore, at a first sight, we do not see much of the tectonics of the study area. Moreover, at a first sight, the results are clearly affected by ionospheric streaks, or orbital un-modeled biases visible as phase modulation stripes whose major axe is parallel to the satellite orbit.

MARSite (GA 308417) D3.4 Deformation map obtained by applying InSAR technique to a sample L-Band SAR dataset

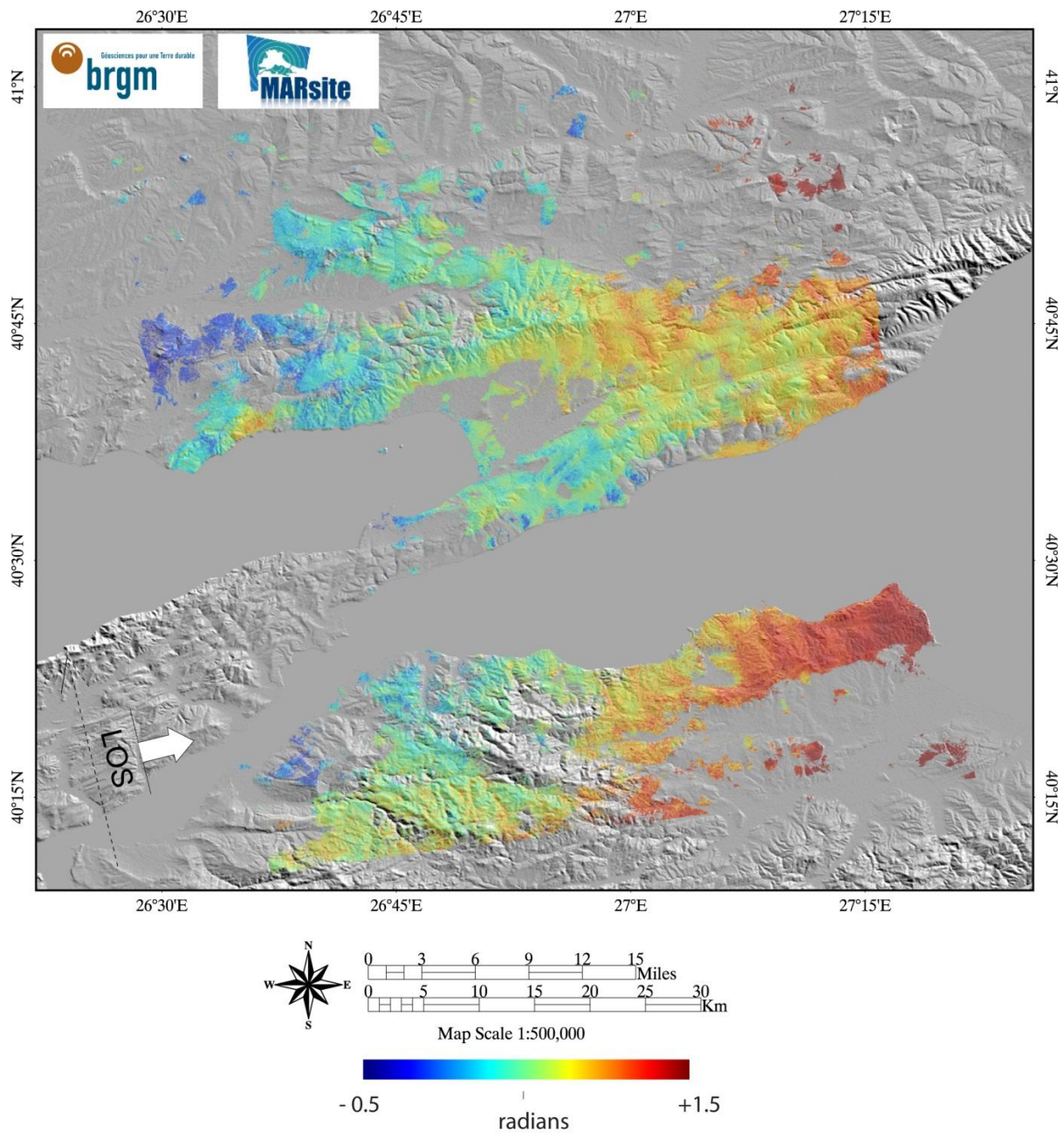


Figure 15. Same as figure 4 but plotted in transparency on the shaded SRTM DEM. The colour scale is in radians / year ; it goes from -0.8 cm/year to 2.7 cm/year.

Also, it seems to us that a residual ramp affects the velocity map. Furthermore, we can notice that some areas are affected by unwrapping errors, particularly where the InSAR measurements are disconnected from the bulk measurements (fig. 8).

We are able to discern a number of local signals (at a kilometeric to sub-kilometeric scale) probably due to land-sliding or other gravitational phenomena on coastal areas.

By plotting the velocity map above a shaded DEM (fig. 7), we cannot see a direct relation between the InSAR velocity map and the topography in the Ganos section of the NAFZ. At the present stage, we can not use the data as they are to make a quantitative interpretation about tectonic motion in the study area. We can notice that a slight offset in the colours across the Ganos fault might suggest dextral shear. This observation is the only encouraging argument to continue the processing work with L-band. Further processing is needed in order to remove the spurious contributions to the InSAR phase and thus highlight the hidden tectonic signal.

### **2.2.3 Discussion**

The tectonic signal within the velocity map retrieved from ALOS Palsar InSAR presented in this report is unfortunately hidden beneath spurious phase contributions. The spurious phase contributions are mainly due to residual orbital errors, a residual phase ramp, the presence of ionospheric disturbances (even if this hypothesis seems to be less and less probable in our opinion, given the regular orientation of the streaks throughout the scene) or some data acquisition biases. We need to investigate this issue further.

In any case, we have to take into considerations that the amount of L-band SAR data was not extraordinary. 13 frames spanning more than 3 years are not so numerous to measure tectonic strain with high level of confidence, considering that the expected tectonic motion, as seen by GPS, is between 0 and 2 cm/year (Ergintav et al., 2012).

Moreover, there have been some registration problems with the image 2007/07/07 probably due to a large difference in the Doppler centroid with respect to the entire stack. So this datum has been discarded (which makes 12 the number of actual Palsar data that we could effectively use for the interferometric analysis).

Further processing is thus foreseen; it mainly consists of better determination of the orbital parameters; defining a strategy for ramp removal; assessing the influence of the ionospheric layer (or other Radio Frequencies Interferences) on the interferograms.

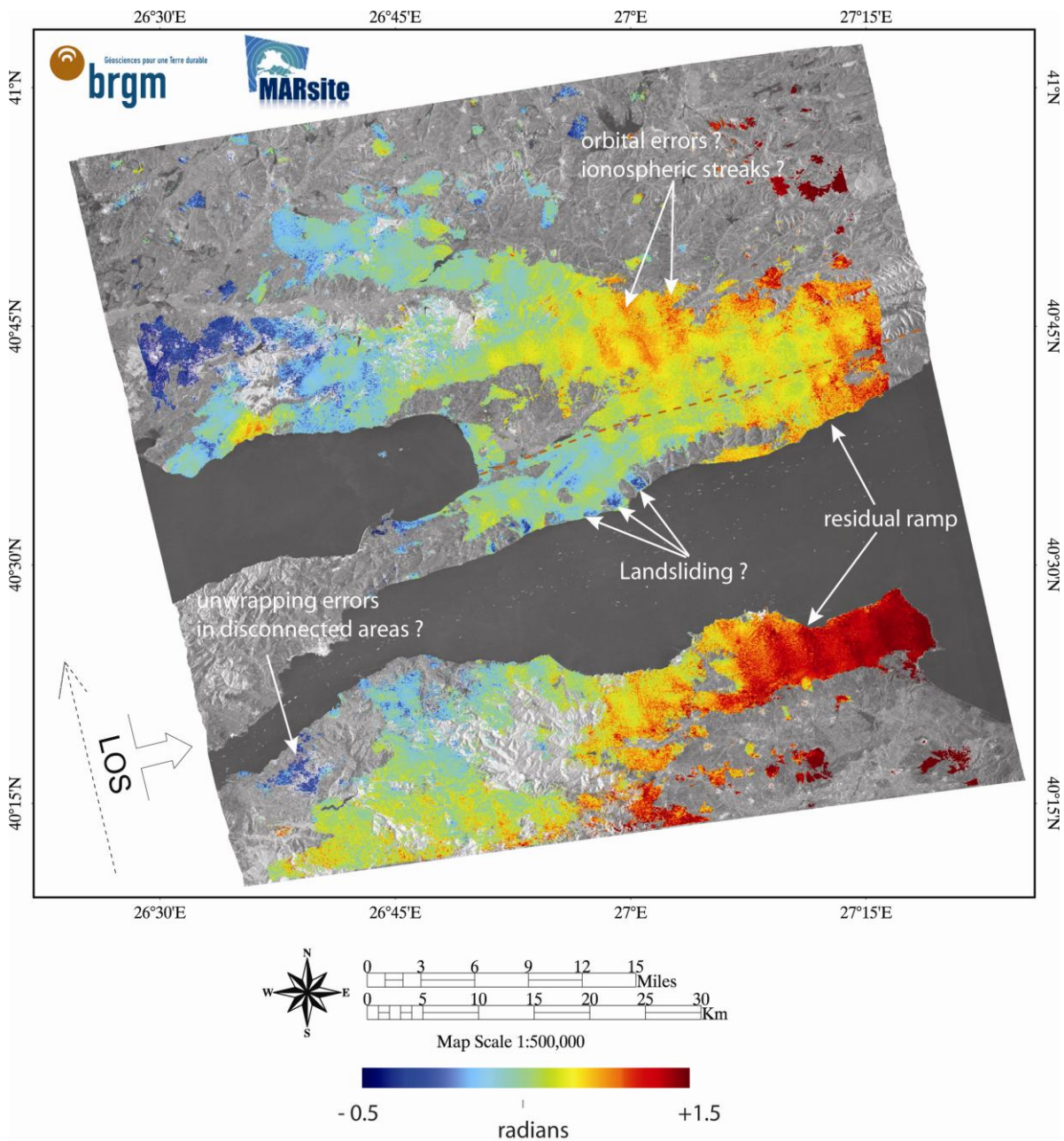


Figure 16. Stack of 45 interferograms with annotation about possible interpretation. The Ganos section of the NAFZ is plotted as a dashed red line. The colour scale is in radians / year ; it goes from -0.8 cm/year to 2.7 cm/year.



## Bibliography

- Aksoy, M.E., Meghraoui, M., Vallee, M., and Cakir, Z., 2010, Rupture characteristics of the A.D. 1912 Murefte (Ganos) earthquake segment of the North Anatolian fault (Western Turkey): *Geology*, 38, 991-994.
- Armijo R., B. Meyer, A. Hubert, A. Barka, Westward propagation of the North Anatolian fault into the northern Aegean: timing and kinematics, *Geology*, 1999, 27, 267–270.
- Armijo R., N. Pondard, B. Meyer, B. Mercier de Lepinay, G. Uçarkus, J. Malavieille, S. Dominguez, M.-A. Gustcher, Beck, N. Çagatay, Z. Cakir, C. Imren, E. Kadir, Natalin, Marmarascarp Cruise party, Submarine fault scarps in the Sea of Marmara pull-apart (North Anatolian Fault): implications for seismic hazard in Istanbul, 2005, *Geochemistry Geophysics Geosystems*, 6, doi: 10.1029/2004GC000896
- Barka A.A., K. Kadinsky-Cade Strike-slip fault geometry in turkey and its influence on earthquake activity, 1988, *Tectonics*, 7, 663–684.
- Berardino P., G. Fornaro, R. Lanari, E. Sansosti, A new algorithm for surface deformation monitoring based on small baseline differential SAR interferograms, *IEEE Trans. Geosci. Remote Sens.*, 2002, 40, 2375–2383.
- Costantini M., P.A. Rosen, A generalized phase unwrapping approach for sparse data, *Proceedings, IGARSS '99, Hamburg, Germany (1999)*, pp. 267–269 June 28–July 2.
- de Michele M., D. Raucoules, F. Rolandone, P. Briole, J. Salichon, A. Lemoine, H. Aochi, Spatiotemporal evolution of surface creep in the Parkfield region of the San Andreas Fault (1993–2004) from synthetic aperture radar, *Earth and Planetary Science Letters*, 2011, 308, 1–2, , 141-150, doi: 10.1016/j.epsl.2011.05.049.
- Doin M.-P., C. Lasserre, G. Peltzer, O. Cavalié, C. Doubre, Corrections of stratified tropospheric delays in SAR interferometry: validation with global atmospheric models, 2009, *J. Appl. Geophys.*, 69 (1), 35–50.
- Elliot J.R., J. Biggs, B. Parsons, T.J. Wright, InSAR slip rate determination on the Altyn Tagh Fault, northern Tibet, in the presence of topographically correlated atmospheric delays, 2008, *Geophys. Res. Lett.*, 35, L12309 doi: 10.1029/2008GL033659.

- Ergintav S., Cakir Z., Dogan U., Cakmak R., Floyd M., King R. W., McClusky S., Reilinger R., Seismic Potential of the North Anatolian Fault in the Sea of Marmara, Turkey, AGU Meeting, December 2014, San Fransisco, USA.
- Janssen C., M. Bohnhoff, Y. Vapnik, E. Görgün, F. Bulut, B. Plessen, D. Pohl, M. Aktar, A.I. Okay, G. Dresen, 2009, Tectonic evolution of the Ganos segment of the North Anatolian Fault (NW Turkey), *Journal of Structural Geology*, 31, 1, 11-28, ISSN 0191-8141, doi:10.1016/j.jsg.2008.09.010.
- Massonnet D., K.L. Feigl Radar interferometry and its application to changes in the earth's surface, *Rev. Geophys.*, 1998, 36, 441–500.
- Meade B.J., B.H. Hager, S.C. McClusky, R.E. Reilinger, S. Ergintav, O. Lenk, A. Barka, H. Özener, 2002, Estimates of Seismic Potential in the Marmara Sea Region from Block Models of Secular Deformation Constrained by Global Positioning System Measurements, *Bull. Seismol. Soc. Am.* 92 , 208–215.
- Motagh M., J. Hoffmann, B. Kampes, M. Baes, J. Zschau, 2007, Strain accumulation across the Gazikoy–Saros segment of the North Anatolian Fault inferred from Persistent Scatterer Interferometry and GPS measurements, *Earth and Planetary Science Letters*, 255, 3–4, 432-444, ISSN 0012-821X, doi:10.1016/j.epsl.2007.01.003.
- Okay A., E. Demirbag, H. Kurt, N. Okay, I. Kuscu, An active, deep marine strike-slip basin along the North Anatolian Fault in Turkey, 1999, *Tectonics*, 18, 129–147.
- Puysségur B., R. Michel, J.-P. Avouac, Tropospheric phase delay in interferometric synthetic aperture radar estimated from meteorological model and multispectral imagery, *J. Geophys. Res.*, 2007, 112, B05419 doi: 10.1029/2006JB004352.
- Reilinger R.E., S. Ergintav, R. Bürgmann, S. McClusky, O. Lenk, A. Barka, O. Gurkan, L. Hearn, K.L. Feigl, R. Cakmak, B. Aktug, H. Ozener, M.N. Töksoz, Coseismic and postseismic fault slip for the 17 August 1999, M=7.5, Izmit, Turkey Earthquake, 2002, *Science*, 289, 1519–1524.

- Tüysüz O., A. Barka, E. Yigitbas, Geology of the Saros graben and its implications for the evolution of the North Anatolian fault in the Ganos-Saros region, *Tectonophysics*, 1998, 293, 105–126.
- Wegmüller U., C.L. Werner, M. Santoro, Motion monitoring for Etna using ALOS PALSAR time series, *Proceedings, ALOS PI Symposium 2009*, November 9–13, Hawaii.
- Werner C., U. Wegmüller, T. Strozzi, Processing strategies for phase unwrapping for InSAR applications, *Proceedings, EUSAR Conference*, June 4–6, Cologne, Germany, unpaginated CD-ROM (2002).
- Zebker H.A., P.A. Rosen, H. Hansley, Atmospheric effects in interferometric synthetic aperture radar surface deformation and topographic maps, *J. Geophys. Res.*, 1997, 102, 7547–7563.